Proceedings of the 2021 Design of Medical Devices Conference
DMD2021
April 12-15, 2021, Minneapolis, MN, USA

DMD2021-1089

HELICAL NEEDLE SUTURE INSERTER PROVIDES INCREASED SUTURE RETENTION FORCE COMPARED TO A STRAIGHT NEEDLE

Etse-Oghena Y. Campbell
Walker Department of Mechanical Engineering,
University of Texas at Austin
Austin, TX

Christopher G. Rylander
Walker Department of Mechanical Engineering,
University of Texas at Austin,
Austin, TX

ABSTRACT

This paper presents an evaluation of the effect of needle geometry on the strength of a tether made using a barbed suture inserted into phantom tissue using a unique device. This tether is designed to secure an intrauterine device (IUD) to uterine fundus, with the aim of improving retention of IUDs inserted in the immediate postpartum period. A factorial experiment was designed to evaluate the effect of needle geometry on tether strength. Tether strength was characterized by the peak retention force of a suture subjected to a uniaxial tensile load. Experiments were performed using phantom tissue. Two needle geometries and three suture sizes were evaluated. Sutures deposited in phantom tissue with the helical needle had up to 132% increase in retention forces compared to sutures inserted with a straight needle, with more advantage at greater active length. The helical needle provides increased suture retention force and is a suitable tether delivery mechanism for this application.

Keywords: Needle, Barbed suture, Suture/tissue pull out test, Tether, Phantom tissue

1. INTRODUCTION

A novel device for inserting and retaining intrauterine devices (IUDs) was developed to improve IUD access and retention in the immediate postpartum (IPP) period. Studies have shown that up to 40% of women who request IUDs are lost during the 6-week waiting period for the uterus to return to its non-pregnant state [1]. However, IPP IUD insertion is a preferred and practical contraceptive solution, as its cost-effective nature for prevention of unplanned pregnancies exhibits an average cost savings ~$282,540 per 1000 women over a 2-year period [2].

The mechanism for improving retention for this application is a temporary tether that would secure an IUD to the uterine fundus through the 6-week puerperium when the uterus returns to its non-pregnant state [3]. Post puerperium, the IUD will be located in close proximity to the uterine fundus, with the central stem completely within the endometrial canal [4]. There is limited data on cervical properties and forces both during childbirth and puerperium [5]. Maximizing the tether's strength within the boundaries of uterine fundus thickness is crucial to withstand the forces the tethered IUD would be subjected to during uterine involution.

The tether used in this application is an intracorporeal absorbable barbed suture. Suture barbs eliminate the necessity of surgical knots required for suture security [6]. A small gauge needle was selected for the tether delivery mechanism. The device will advance the needle point into tissue, concurrently inserting a barbed suture into the tissue. Upon retracting the needle, surrounding tissue will relax around suture barbs, anchoring the suture in the space delineated by the needle, and providing a tether for the IUD.

Previous studies on barbed suture technology have focused on determining how angle and cut depth of barbs on a suture affect tissue anchoring properties, with the aim of optimizing barb geometry for skin and tendon tissues [7]. However, this work aims to adapt existing barbed suture technology for use in a unique inserter device.

This work focused on the method of tether attachment and not the application. Our primary interest is tether strength. Factors which may impact this strength include: barb geometry, suture material properties, surrounding tissue properties and needle geometry. The primary objective of this study was to analyze the impact of needle geometry on the strength of a suture tether made by inserting a barbed suture into phantom tissue. A two-factorial design of experiments was developed for this study. Suture samples were prepared from a monofilament barbed suture, and two needle geometries were evaluated. Results from this work provided data which informed selection of suitable needle geometry for an IUD delivery device.

2. MATERIALS AND METHODS

2.1 Prototype Design

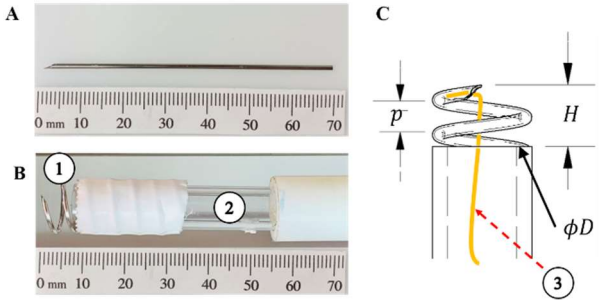

FIGURE 1. NEEDLE PROTOTYPES: A. STRAIGHT NEEDLE, B. HELICAL NEEDLE, C. HELICAL NEEDLE DIMENSIONS (1) HELICAL NEEDLE, (2) RIGID POLYCARBONATE TUBE (3) BARBED SUTURE THREADED INTO HELICAL NEEDLE

Two needle geometries were selected, a straight needle and a helical needle, shown in Figure 1. Prototypes for both geometries were made from polished 304 stainless steel tubing (OD 1.27 mm × ID 0.84 mm). For the straight needle, tubing was cut to a length of 70 mm. The helical needle was cold formed into a right-handed helix with diameter, ϕD=10 ± 0.04 mm and pitch, p = 5 ± 0.09 mm. Helix pitch was selected such that one revolution would advance the needle tip p mm along the helix's axis. The diameter was constrained by cervical dilation dimensions and restricted to no more than 15 mm, and the total height H is limited to 10 mm by postpartum fundal thickness. One end of the helical needle was fixed on a rigid polycarbonate tube and the other end was ground to a 3.7 mm bevel needle point.

2.2 Material Selection & Preparation

Three sizes, 3-0-, 2-0- and 0-gauge, of Covidien V-Loc™ 90-day absorbable suture, were used. 70 mm lengths of the monofilament suture were prepared, and 10 mm of the length was marked with permanent dye, then threaded into the needle (Figure 1).

For the tissue phantom, open-cell soft polyurethane (PU) foam was selected to simulate the mechanical and fibrous properties of soft tissue [6]. The PU foam was cut into square samples 60 mm long × 60 mm wide × 17 mm thick, then placed in a custom tissue holder for the experiments.

2.3 Experimental Design

Two variables were manipulated for this study: suture size and needle tip displacement. Three levels for each variable were selected. The two-variable, three-level factorial experimental design is shown in Table 1, and was executed for both straight and helical needle geometries.

TABLE 1. EXPERIMENTAL DESIGN SUMMARY

Needle tip displacement	Suture size (d gauge)		
(z mm)	3-0	2-0	0
15 mm	×	×	×
20 mm	×	×	×
25 mm	×	×	×

Needle tip displacement is defined along the needle's trajectory. This displacement is controlled by an Instron for the straight needle, and by a stepper motor setup for the helical needle

2.4 Experimental Procedure

The experiment was conducted in two stages: suture insertion and tether strength testing.

2.4.1 Suture Insertion

An Instron Electropuls™ E1000 universal testing machine, shown in Figure 2, guided the prepared straight needle into the phantom tissue. The needle was fixed in the intron's upper jaws, which are fixed to a 2kN load cell on the Instron's crosshead. The tissue phantom in its holder was secured on the Instron base using a custom mount. The needle's motion was restricted to the z-axis and controlled by using Instron Wavematrix™ software. The needle was advanced to a zero-position in near-contact with the phantom tissue's surface. The needle was driven z mm (Table 1) into phantom tissue at a constant rate of 0.5 mm/sec. Then, needle's motion was reversed through a distance of $z + 5$ mm, which allowed surrounding phantom tissue to relax around suture barbs, and anchor the suture in phantom tissue. The axial force was measured and recorded in the direction of motion. The suture was marked at the point of insertion using a dye.

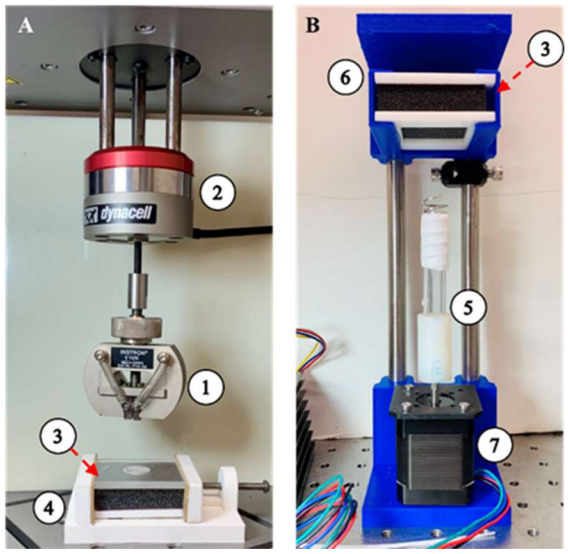

FIGURE 2. SETUP FOR SUTURE INSERTION A. STRAIGHT NEEDLE, B. HELICAL NEEDLE: (1) UPPER JAWS, (2) 2 KN LOAD CELL, (3) PHANTOM TISSIE AND TISSUE HOLDER (4) TISSUE MOUNT, (5) HELICAL NEEDLE AND COUPLER (6) VERTICAL STAGE (7) STEPPER MOTOR

The helical needle was guided into phantom tissue using the stepper motor assembly in Figure 2. The needle's polycarbonate tube was coupled to the stepper motor's shaft, and phantom tissue was secured in a 1-degree-of-freedom vertical stage. The vertical stage was lowered to a position in near-contact with the needlepoint. Preliminary experiments had determined that in addition to needle rotation, a force co-axial

with the helix axis was necessary to facilitate tissue puncture and subsequent cutting through the tissue. A 4.9 N axial force was applied by placing calibration masses on the vertical stage. The motor shaft rotated the helical needle clockwise through an angle θ corresponding to needle tip displacement, z (TABLE 1) at a constant rate of 1 mm/sec using an Arduino Uno. After which, the needle's motion was reversed through a distance $z + 5$ mm, to ensure the needle tip was completely disengaged from phantom tissue. Upon reversal, the barbed suture tether was deposited in the phantom tissue. Insertion force was not recorded for the helical needle. The suture was marked at the juncture where it emerged from the phantom tissue surface using a dye agent (Figure 3).

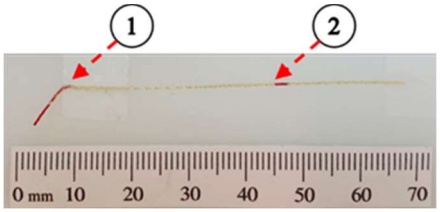

FIGURE 3. BARBED SUTURE AFTER TETHER STRENGTH TEST. (1) INITIAL ANCHOR POSITION (2) JUNCTURE WHERE SUTURE EMERGES FROM PHANTOM TISSUE

2.4.2 Tether strength test

The phantom tissue holder was secured on the Instron base, and the suture's free end was secured in its jaws. Uniaxial tensile loading to failure for N= 9 replicates (N=4 for helical needle) was conducted using the Instron Electropuls™ E1000 universal testing machine at a rate of 0.5 mm/s. Tether strength was estimated by retention force, defined as the peak force observed during the uniaxial tensile loading test. Failure was defined as the first of two occurrences:1) suture fracture or 2) suture disengagement from the tissue. Force and displacement in the direction of motion were recorded for straight and helical needles. The length of suture deposited, defined as the active length, L_A, is the displacement between initial anchor point and the point where suture emerges from the tissue as shown in Figure 3.

3. RESULTS AND DISCUSSION

The 25 mm needle tip displacement and 0-gauge suture resulted in higher L_A, suggesting that the length of suture deposited in tissue, L_A, is dependent on needle tip displacement into phantom tissue. It is important to note that although the needle tip was driven some displacement z mm into phantom tissue, the deformation, creep and relaxation that characterize viscoelastic properties open cell PU foam prevent exactly z mm of suture from being deposited in the tissue phantom.

Figure 4 plots retention force, F_R, as a function of active suture length for the three suture sizes tested for the straight and helical needles. Data was best fit by a linear curve fit of the form

$$f(x) = p_1 x + p_2 \quad (1)$$

R^2 values for the curve fit for 3-0-, 2-0- and 0-gauge

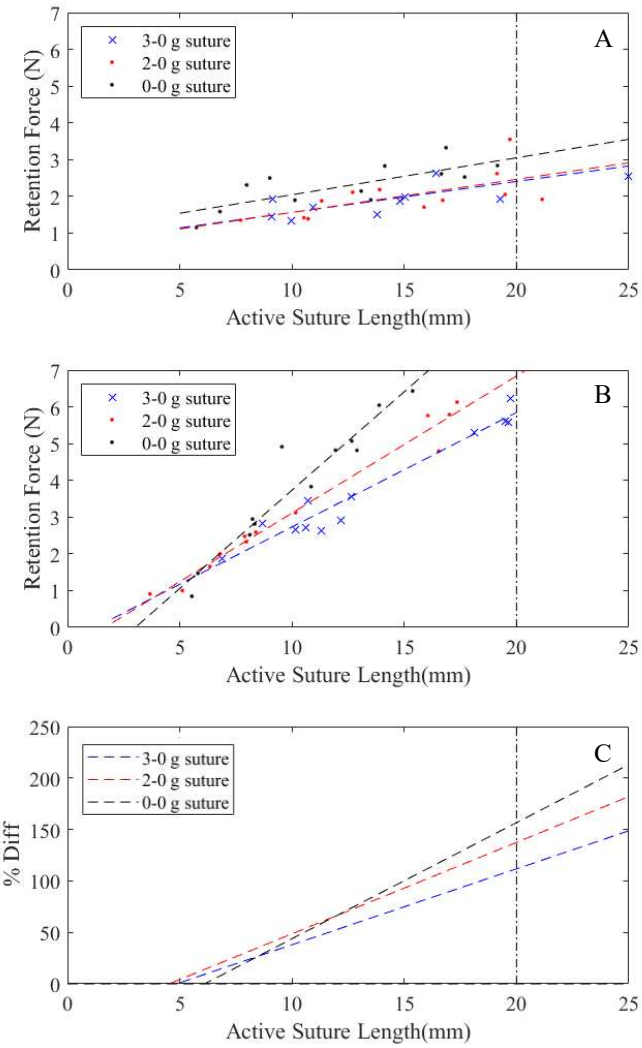

FIGURE 4. RETENTION FORCE VS ACTIVE LENGTH FOR: A. SUTURE TETHERS FOR STRAIGHT NEEDLE, B. HELICAL NEEDLE, C. % $Diff$ BETWEEN STRAIGHT AND HELICAL NEEDLE RETENTION FORCE VS ACTIVE LENGTH

sutures inserted using the straight (helical) needle are 0.73, 0.518 and 0.697 (0.94, 0.98 and 0.92) respectively. Figure 4 shows that the gradient of the curve fit for the helical needle is greater than that of the straight needle for the same active length. For emphasis, the percentage difference between the retention force of the straight needle ($F_{R,S}$) and that of the helical needle ($F_{R,H}$) for active length L_A was computed using Equation 2.

$$\%\ Diff = \frac{F_{R,H} - F_{R,S}}{F_{R,S}} \times 100 \quad (2)$$

Figure 4C shows the % $Diff$ increasing with increasing L_A for the three suture sizes, suggesting that needle and suture trajectory within the phantom and active length has a significant effect on tether strength.

The mechanism of failure for all trials was suture disengagement. However, for sutures inserted using the helical

needle, the phantom tissue sheared compared to the straight needle, where the suture retracted from the vertical hole created by the needle. A uniaxial tensile force was used for the tether strength test for both insertions (straight and helical insertions). The tensile force direction is coaxial to the barbed suture's trajectory in phantom tissue for the straight needle. Upon loading, the suture is extracted through the hole created by the needle. The tensile force direction is tangent to the barbed suture's trajectory in phantom tissue for the helical needle, and the future is embedded beneath tissue layers. Upon tensile loading, the barbed suture was observed to shear the phantom tissue.

The 0-gauge suture had the largest diameter (0.4 ± 0.01 mm) compared to the 2-0 and 3-0 sutures (0.3 ± 0.01 mm and 0.2 ± 0.01 mm respectively), and consistently resulted in high retention forces compared to the other two suture sizes, despite all suture barbs having the same dimensions. One possibility is that the suture body and barbs of the 0-g suture made more direct contact with surrounding tissue, thus improving the anchoring mechanism. Because all sutures used in this study were deposited in tissue using the same needle. This may not be ideal in practice because the needle created the same sized hole regardless of the suture size. In [7], needle size was optimized for a single suture size.

Figure 5 shows a sample of axial force data against needle displacement recorded for a 2-0 suture deposited in phantom tissue using the straight needle. Tissue puncture is identified by a peak in force followed by a sudden decrease [8]. Puncture forces for the 3-0-, 2-0- and 0-gauge sutures were 4.015 ± 0.39 N, 4.651± 0.55 N and 6.112 ± 0.614 N respectively. This is to be expected because the 0-gauge suture has the largest diameter. Consecutive variations in force have been identified by [8] as a combination of friction forces between tissue phantom and needle contact interfaces, cutting forces, and internal tissue stiffness. This may explain why the 0-gauge suture had relatively shorter active suture lengths compared to the 2-0 and 3-0 sutures. This study did not characterize force components after puncture.

This project is a work in progress. For the straight needle, R^2 values of the linear fit indicate that other factors not considered in this study may impact tether strength and the effectiveness of the tether delivery mechanism. A more detailed statistical analysis should be conducted on this data to better understand the mechanisms of tissue, needle, and barbed suture interaction.

Pain levels from insertions performed using a helical needle are not expected to differ from insertions performed using a straight needle from a recipient's perspective, primarily because the procedure is expected to be performed within the hour following delivery.

Improved tether retention with the helical needle is a promising result because fundal thickness is limited to 10 mm, thus insertion depth is also limited so as to not perforate the uterus. With the helical needle geometry, longer suture lengths may be deposited in fundal tissue, thus increasing tether strength and reducing the incidence of tether failure by suture disengagement.

4. CONCLUSION

This work focused on a method of tether attachment in uterine tissue. This study demonstrated that suture tether strength is significantly improved when the helical needle is used to deposit suture in tissue. More work is required to thoroughly characterize factors that affect suture deposition and consequently impact retention force.

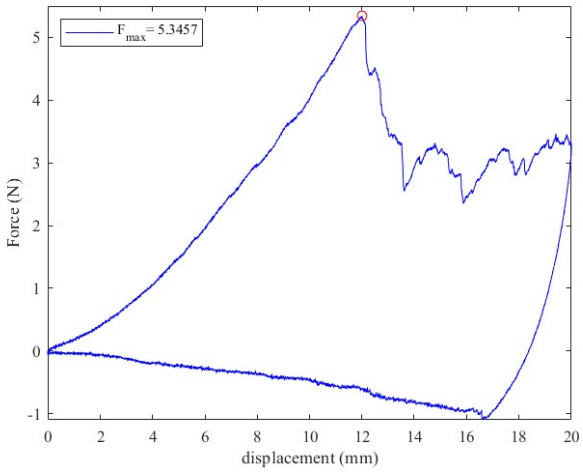

FIGURE 5. AXIAL FORCES MEASURED DURING INSERTION STAGE FOR STRAIGHT NEEDLE. TISSUE PUNCTURE OCCURS AT F_{MAX}

Future work will include a parametric redesign to optimize helix dimensions for different sized sutures so as to improve efficiency of depositing suture in tissue, and validating the results in ex-vivo biological tissue.

REFERENCES

[1] J. A. Ogburn, E. Espey, and J. Stonehocker, "Barriers to intrauterine device insertion in postpartum women," *Contraception*, vol. 72, no. 6, pp. 426–429, 2005, doi: 10.1016/j.contraception.2005.05.016.

[2] C. I. Washington, R. Jamshidi, S. F. Thung, U. A. Nayeri, A. B. Caughey, and E. F. Werner, "Timing of postpartum intrauterine device placement: A cost-effectiveness analysis," *Fertil. Steril.*, vol. 103, no. 1, pp. 131–137, 2015, doi: 10.1016/j.fertnstert.2014.09.032.

[3] E. Campbell, C. G. Rylander, L. Thaxton, and M. Y. Williams-Brown, "Novel method and device for delivery and retention of intrauterine devices in the immediate postpartum period: Pilot baboon feasibility study," in *Frontiers in Biomedical Devices, BIOMED - 2020 Design of Medical Devices Conference, DMD 2020*, 2020, pp. 7–9, doi: 10.1115/DMD2020-9049.

[4] H. E. Boortz, D. J. A. Margolis, N. Ragavendra, M. K. Patel, and B. M. Kadell, "Migration of intrauterine devices: Radiologic findings and implications for patient care," *Radiographics*, vol. 32, no. 2, pp. 335–352, 2012, doi: 10.1148/rg.322115068.

[5] A. Paskaleva, "Biomechanics of cervical function in

pregnancy : case of cervical insufficiency," 2008.
[6] J. Leung, G. L. Ruff, and M. A. Megaro, "Barbed, bi-directional medical sutures: Biomechanical properties and wound closure efficacy study," in *2002 Society for Biomaterials 28th Annual Meeting Transactions*, 2002, vol. 724.
[7] N. P. Ingle and M. W. King, "Optimizing the tissue anchoring performance of barbed sutures in skin and tendon tissues," *J. Biomech.*, vol. 43, no. 2, pp. 302–309, 2010, doi: 10.1016/j.jbiomech.2009.08.033.
[8] A. M. Okamura, C. Simone, and M. D. O'Leary, "Force Modeling for Needle Insertion Into Soft Tissue," *IEEE Trans. Biomed. Eng.*, vol. 51, no. 10, pp. 1707–1716, Oct. 2004, doi: 10.1109/TBME.2004.831542.